Confinement-Induced Transition of Topological Defects in Smectic Liquid Crystals: From a Point to a Line and Pearls

Joonwoo Jeong and Mahn Won Kim*

Department of Physics, KAIST, Daejeon, 305-701, Republic of Korea

(Received 17 November 2011; revised manuscript received 1 March 2012; published 18 May 2012)

We report a study on the confinement-induced transition of the topological defects of liquid crystals (LCs) using smectic-*A* LCs confined in prolate spheroids with homeotropic anchoring. Upon increasing the aspect ratio of a LC droplet, dispersed in a stretched elastomer film, the topological defect undergoes a transition from a point to a line of which the length is a function of the aspect ratio. Additionally, when the size of a droplet is larger than a certain value, the defect has a pearl-necklace-like texture. We propose a simple model to understand the formation of these defects in terms of the misorientation and undulation instability of the smectic layers.

DOI: 10.1103/PhysRevLett.108.207802 PACS numbers: 61.30.Jf, 61.30.Eb, 61.30.Pq

A balance between bulk elasticity and surface anchoring usually determines the structure of confined liquid crystals (LCs) [1]. With a typical elastic modulus of $\sim 10^{-11}$ N and a surface anchoring coefficient of $\sim 10^{-5}$ N/m, confinements on the micron scale affect the structure of LCs greatly and often produce topological defects [2–4] which can be observed optically. Understanding and controlling these defects are related to various topics in condensed matter physics [5]. They are also important in technological applications such as quality control of LC-based products and the recently suggested lithography using LCs [6,7].

The size and shape of the confinements are critical to obtaining specific topological defects of LCs. For example, size-dependent changes in LC ordering have been clearly observed in LC droplets [8,9]. In polymer-dispersed liquid crystal (PDLC) research, how the shape of LC droplets dispersed in a polymer matrix affects the electro-optic properties has been studied [10–12]. Many other geometries with controlled surface polarities have been studied as confinements [13–23]. However, there has been no systematic observation of individual defects in confinements of low symmetry with continuously varying curvature. In addition, the transition of topological defects due to continuous changes in the shape of the confinements has not been reported.

In this Letter, we observe the transition of topological defects of smectic-*A* (Sm-*A*) LCs confined in prolate spheroids with homeotropic anchoring while controlling systematically the shape and size of the confinements. We choose a prolate spheroid in which three radii, a, b, and c, have $a > b = c$, because it has a continuously varying curvature and we can control its shape by the unidirectional stretching of a spherical droplet [10,24,25]. This simple but nontrivial geometry can be considered as a type of intermediate geometry between a sphere ($a = b = c$) and a cylinder ($a = \infty$, $b = c$).

To implement this, we utilize 4'-octyl-4-biphenylcarbonitrile (8CB) droplets dispersed in poly(dimethylsiloxane) (PDMS) elastomer, which is known to induce homeotropic anchoring [11]. The LC-in-PDMS film of 130 μm thickness is mounted on a custom-built tensile tester which stretches the film unidirectionally using a micrometer. We track a chosen set of LC droplets while stretching the film under an optical microscope. All images are taken with quasimonochromatic light (wavelength $\approx$ 560 nm) from a halogen lamp using a bandpass filter (BP 545–580, Olympus). To obtain the equilibrium configurations of the LC droplets, after being stretched, the film is heated over the smectic *A*-nematic transition point and cooled back to the ambient temperature, at which 8CB is in Sm-*A* phase. All the observations in the Sm-*A* phase are done at the ambient temperature of 26 $\pm$ 1.5 °C.

As shown in Fig. 1, images from one droplet are collected according to the aspect ratio and the LC phase. Polarized optical microscopy (POM) images are also taken with two different directions of crossed polarizers. By fitting the bright-field images of the droplets into ellipses, we measure the length of the major and minor axes according to the strain of the film. The maximum strain is limited by the rupture of the film. To quantify this strain in terms of the droplets' dimensions, we define the aspect ratio as the ratio of the major axis to the minor axis. The volume of this spheroidal cavity in PDMS, which is filled with LCs, is measured and maintained within 5% experimental error. This small error is deemed feasible because the Poisson's ratio of PDMS is close to 0.5 [26].

It is clear from Fig. 1(a) that the defect of Sm-*A* LC is strongly affected by the confinement shape. When the aspect ratio is 1, the dark spot of a point defect in the bright-field image and the Maltese crosses according to the direction of the crossed polarizers can be identified. Upon increasing the aspect ratio of the LC droplet in the Sm-*A* phase, the dark spot at the center in the bright-field image appears to extend into a line. This line corresponds to the dark line on the major axis in the POM images. The other

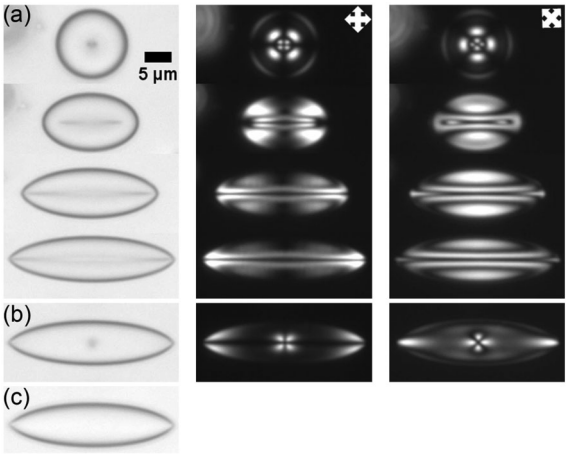

FIG. 1. Optical microscopy images of an identical LC droplet according to the aspect ratio and LC phase. (a) Smectic-*A* phase. The first column contains the bright-field images. The second and third columns show the POM images. The directions of crossed polarizers are shown as arrows in the upper right corners. The same format applies to (b) and (c). (b) Nematic phase. (c) Isotropic phase. POM images of the isotropic phase are omitted due to the lack of birefringence.

dark regions in the POM images can be matched to regions where the retardation of quasimonochromatic light is equal to 2π or where the local director field is aligned parallel to either the polarizer or analyzer [11]. In the nematic phase [Fig. 1(b)], we simply observe the point defect, and thereby the Maltese crosses. The isotropic phase does not show any defects or birefringence [Fig. 1(c)].

We identify the dark line on the major axis as a line defect. This line defect always appears dark under the rotation of crossed polarizers [27]. The length of the line defect is plotted with points in Fig. 2(a) according to the aspect ratio and the diameter of an original spherical droplet. In Fig. 2(b), to compare these lengths regardless of the sizes of the droplets, the lengths are normalized to the major axis $2a$. We measure the lengths 5 times and omit error bars because the sample standard deviations of most data points are less than 4%. We change the phase of the LC into the nematic phase and cool the sample back to the Sm-*A* phase before each measurement.

Under the assumption that smectic layers of the same thickness are parallel to each other and to the interface, directors of LC molecules lie on the normal lines to the nearest boundary due to homeotropic anchoring [28]. If we consider the first quadrant of a spheroid, as shown in Fig. 3(a), these normal lines intersect the major axis at angles θ with the x intercepts $(x', 0)$. From the equation of the ellipse $x^2/a^2 + y^2/b^2 = 1$ and the equation of a line normal to the ellipse at (X, Y), x' is determined by Eq. (1) when $a^2Y/b^2X = \tan\theta$ [27],

$$\frac{x'}{a} = \frac{a/b - b/a}{\sqrt{\tan^2\theta + (a/b)^2}}. \quad (1)$$

When $(x', 0)$ moves from $(a, 0)$ to $(0, 0)$, θ increases from 0° to 90°. Note that θ is 0° from $(a, 0)$ to $((a^2 - b^2)/a, 0)$, which is the center of curvature at $(a, 0)$ of the ellipse.

Because of these misorientation angles θ, parallel smectic layers of the same thickness cannot fill the prolate spheroid. In other words, as shown in Figs. 3(b) and 3(c), smectic layers around the major axis are bent through 2θ and thus become dilated, $d_d > d_0$, or create defects. When K is the splay modulus and B is the compressional (dilational) modulus of Sm-*A* LC, the penetration length $\lambda = \sqrt{K/B}$ is comparable to the thickness of one smectic layer $d_0 \sim 2$ nm. Then, considering the thickness of the curvature wall $t_{CW} \sim 2\lambda/\tan\theta$ [29], we assume that the dilated region is very small compared to the size of the droplet, $t_{CW} \ll a$. When $\theta \ll 1$ rad, the dilation is also very small. Therefore, Eq. (1), which assumes parallel smectic layers of the same thickness, can be valid at the micron scale.

We assume that the dilation of smectic layers in the misoriented region plays a major role in the formation of the line defect. As the misorientation angle θ increases from 0°, the elastic free energy of the configuration shown in Fig. 3(b) increases rapidly due to the dilation [29]. When θ surpasses a critical misorientation angle γ, smectic

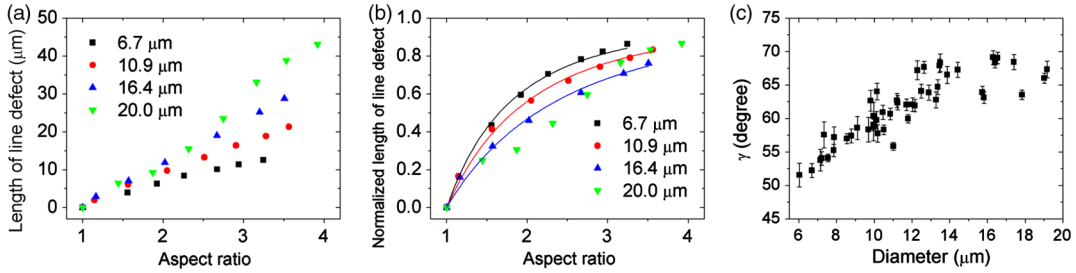

FIG. 2 (color online). The lengths of line defects and the critical angle γ according to the aspect ratios and the diameters of the original spherical droplets. (a) The lengths of line defects of four representative droplets are plotted with points. (b) The lengths of (a) are normalized to the major axes at each aspect ratio. Solid lines are fitting results using Eq. (1) when $x' = l/2$ and $\theta = \gamma$. (c) The critical angles γ are plotted with points according to various diameters of 48 original spherical droplets. Each γ is obtained from the fitting like a solid line in (b).

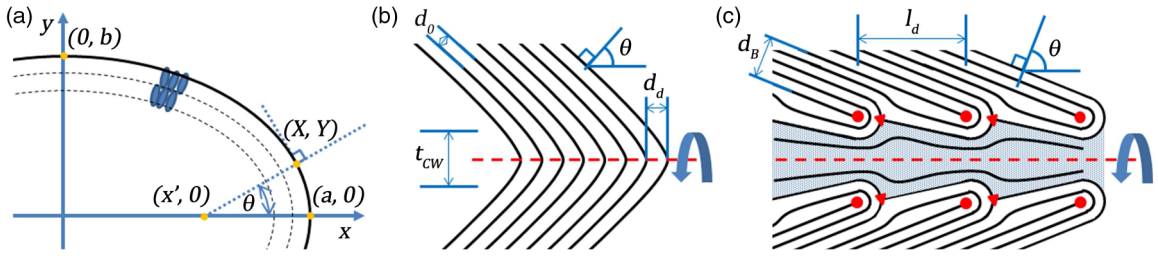

FIG. 3 (color online). Schematic diagrams of smectic layers in the cross section of a prolate spheroid. (a) The first quadrant of the cross section that shows parallel smectic layers with homeotropic anchoring. Cigar-shaped rods represent LC molecules. The thickness of the smectic layers is not in the actual scale. (b) The dilated smectic layers when $\theta < \gamma$. A magnified view of one misoriented region on the x axis of (a). The thick rotating arrow represents the axial symmetry. d_0 is the thickness of one smectic layer without dilation, d_d the thickness of one smectic layer with dilation, and t_{CW} the thickness of the dilated region. (c) The smectic layers with defects when $\theta > \gamma$. The dashed line and the circular and triangular dots represent disclinations. The shaded area around the dashed line emphasizes the undulation of layers. d_B is the size of the Burgers vector, and l_d is the distance between two edge dislocations.

layers can lower the elastic free energy by creating defects. In other respects, when $(x', 0)$ moves from $(a, 0)$ to $(0, 0)$, the dilation $d_d - d_0$ increases and accumulates. When this integrated dilation becomes comparable to the critical thickness [30,31], smectic layers can break into the defects [32].

Assuming that γ is mainly determined in the misoriented region localized around the major axis, we reason that γ is independent of the shape of the droplet, in other words, the aspect ratio. Then, using Eq. (1), we estimate the critical misorientation angle γ, where the line defect starts to appear. When l is the length of the line defect and $x' = l/2$, $\theta = \gamma$, Eq. (1) becomes the relation between the aspect ratio (a/b) and the normalized length of the line defect $(l/2a)$ with only one parameter, the critical misorientation angle γ. The solid lines in Fig. 2(b) are the fitting results to provide γ using this relation.

It is worthwhile to note that γ depends on the size of the original spherical droplets. As shown in Fig. 2(c), γ lies between 50° and 70° depending on the size of the original spherical droplets. In Fig. 2(c), the error bars are from the standard errors of fittings. We cannot measure reliably the length of the line defect when the diameter of the droplet is smaller than 6 μm. On the other hand, when droplets exceed 20 μm in diameter, the data start to deviate remarkably from the fitting function, as shown with inverse triangles in Fig. 2(b). Our model seems to be invalid for large droplets. When the diameter is as large as 40 μm, a line defect even evolves into a complex periodic texture, resembling a pearl necklace, as shown in Fig. 4.

In fact, similar misoriented regions have been studied as singular lines in focal conic domains [33–35]. Only de Gennes calculated the approximate elastic free energy per unit length of this singular line with a very small and constant misorientation angle [2,33]. In addition, de Gennes suggested the configuration of a large $\theta \sim 1$ rad, which we draw explicitly in Fig. 3(c). It consists of an array of edge dislocations with axial symmetry. One edge dislocation decomposes into a pair of circular disclination lines, as represented by circular and triangular dots. In addition, the dashed line along the rotational axis represents the singular disclination. However, calculating the elastic free energy of these configurations of arbitrary θ is a challenging problem.

To gain insight into the formation of the line defects, we introduce a simplified two-dimensional (2D) elastic free energy model in the cross sections, as shown in Figs. 3(b) and 3(c) This is very similar to the calculations in the literature which compared the elastic free energy of a curvature wall and a dislocation wall [36,37]. Assuming a slowly varying θ along the major axis, the elastic free

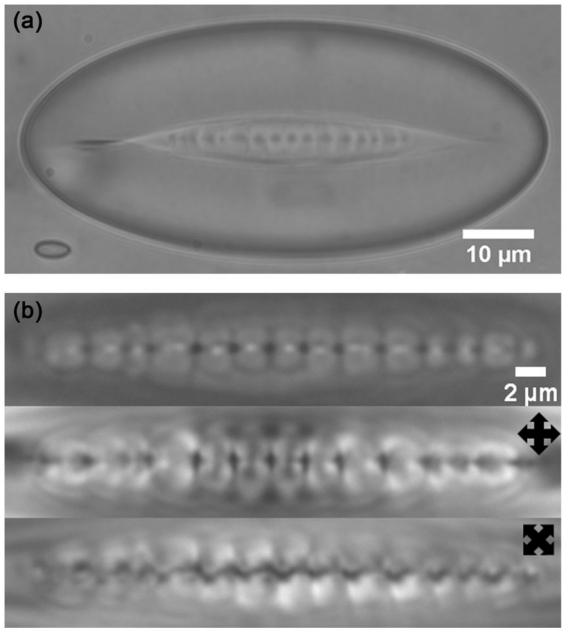

FIG. 4. Optical microscopy images of one large LC droplet. (a) A bright-field image of an elongated large LC droplet in the Sm-A phase. (b) Bright-field and POM images of the magnified central region of (a). The first row is the bright-field image. The second and third rows show the POM images. The black arrows show the directions of the crossed polarizers.

energy per unit area of the curvature wall in Fig. 3(b) is given by Eq. (2) [29],

$$E_{\mathrm{CW}} = 2\sqrt{KB}\cos\theta(\tan\theta - \theta). \quad (2)$$

The elastic free energy per unit area of the configuration shown in Fig. 3(c) can be estimated as the elastic free energy per unit length of an isolated edge dislocation divided by the distance between dislocations l_d [38]. The elastic free energy per unit length of an isolated edge dislocation is given by Eq. (3) [2], where d_B is the size of the Burgers vector of the edge dislocation and d_0 is the thickness of one smectic layer,

$$W = \frac{B\lambda d_B^2}{2\xi} + \frac{\pi K}{2}\ \ln\frac{d_B}{2d_0} + \tau_c. \quad (3)$$

$\xi \sim d_B/2$ is the radius of the core, which is used as the cutoff length during the integration of the elastic free energy. τ_c is the core energy that cannot be described using the continuum elastic free energy model; it is of the order of K [1]. Equation (3) can be written as $\alpha B\lambda d_B$, where $\alpha = [1 + \frac{\pi\lambda}{2d_B}\ \ln(\frac{d_B}{2d_0}) + \frac{\lambda}{d_B}]$. We have the numerical constant $\alpha \approx 1$ for $d_B \gg \lambda$ and $\alpha \approx 1.5$ for $d_B \sim 2\lambda$. Because there are two edge dislocations ($y > 0$ or $y < 0$) along $l_d = d_B/\cos\theta$, the elastic free energy per unit area is finally given by Eq. (4) when $d_B \gg \lambda$ [39],

$$E_{\mathrm{DW}} = 2W/l_d \approx 2\sqrt{KB}\cos\theta. \quad (4)$$

By equating Eq. (2) with (4), we can estimate the critical misorientation angle $\gamma \approx 65°$ at which the elastic free energy of these two configurations becomes comparable in 2D. Although it is notable that the theoretical estimation lies within the range of experimental data, this model does not explain the size dependency of γ shown in Fig. 2(c). This is probably because this simplified estimation in 2D does not consider the 3D aspects of defects such as the axial disclination and the negative Gaussian curvature in Fig. 3(c). The contribution of 3D defects to the simple 2D model is roughly estimated in the Supplemental Material [27].

To explain the unique structure of large droplets, the undulation of the smectic layers with axial symmetry needs to be considered [40–43]. Cladis first observed a beaded texture induced by the undulation instability of Sm-A LCs in a cylindrical confinement. In Fig. 4, this pearl-necklace-like defect is similar to the beaded texture. Even the repeat period of the texture is similar to the reported theoretical estimation $2\pi\sqrt{2R\lambda} \approx 1.8\ \mu$m, where the radius R of a cylindrical confinement is about 20 μm and the penetration length $\lambda = \sqrt{K/B}$ of a typical Sm-A LC is about 2 nm.

We propose that the undulation in our experiment results from the periodic defect structure shown in Fig. 3(c). The shaded cylindrical core undergoes periodic dilation between the edge dislocations. If the size of the Burgers vector and the misorientation angle are large enough, the largely undulated cylindrical core may break into the periodic defects. This is supported by our observation of these defects shown only in the central region, where the misorientation angle is close to 90°. To confirm this defect structure, we are planning additional experiments such as electron microscopy of cross-sectioned samples.

In summary, we observe the transition of the topological defects of LC while controlling the shape of confinements *in situ* with different confinement sizes. This system offers an unprecedented example which will enhance our understanding of defects due to continuously varying misorientations imposed by confinement. Simultaneously, our results show that we can expand the controllability of the structure of LCs using simple but nontrivial confinement types such as a prolate spheroid. The line defects or periodic textures tunable by the shape and size of the confinement may offer intriguing possibilities for applications. Additionally, this type of spheroidal confinement, even with other surface anchoring options, is applicable not only to other LCs but also to other organic and soft materials.

This work was supported by World Class University Program (R33-2008-000-10163-0) and Basic Science Research Program (2009-0087691) through the National Research Foundation of Korea funded by the Ministry of Education, Science, and Technology. This work was also supported by the Brain Korea 21 projects by the Korean government.

*mwkim@kaist.ac.kr

[1] M. Kleman and O. D. Lavrentovich, *Soft Matter Physics: An Introduction* (Springer, New York, 2002).
[2] M. Kléman, *Points, Lines, and Walls: In Liquid Crystals, Magnetic Systems, and Various Ordered Media* (John Wiley & Sons, New York, 1982).
[3] M. Kleman, Rep. Prog. Phys. **52**, 555 (1989).
[4] O. D. Lavrentovich, Liq. Cryst. **24**, 117 (1998).
[5] T. C. Lubensky, D. Pettey, N. Currier, and H. Stark, Phys. Rev. E **57**, 610 (1998).
[6] D. K. Yoon, M. C. Choi, Y. H. Kim, M. W. Kim, O. D. Lavrentovich, and H.-T. Jung, Nature Mater. **6**, 866 (2007).
[7] Y. H. Kim, D. K. Yoon, H. S. Jeong, O. D. Lavrentovich, and H.-T. Jung, Adv. Funct. Mater. **21**, 610 (2011).
[8] A. Golemme, S. Zumer, D. W. Allender, and J. W. Doane, Phys. Rev. Lett. **61**, 2937 (1988).
[9] J. K. Gupta, S. Sivakumar, F. Caruso, and N. L. Abbott, Angew. Chem., Int. Ed. **48**, 1652 (2009).
[10] I. Amimori, N. V. Priezjev, R. A. Pelcovits, and G. P. Crawford, J. Appl. Phys. **93**, 3248 (2003).
[11] P. S. Drzaic, *Liquid Crystal Dispersions* (World Scientific, Singapore, 1995).
[12] D. A. Higgins, Adv. Mater. **12**, 251 (2000).
[13] M. C. Choi, T. Pfohl, Z. Wen, Y. Li, M. W. Kim, J. N. Israelachvili, and C. R. Safinya, Proc. Natl. Acad. Sci. U.S.A. **101**, 17340 (2004).

[14] G. P. Crawford and S. E. Zumer, *Liquid Crystals in Complex Geometries: Formed by Polymer and Porous Networks* (Taylor & Francis, London, 1996).
[15] A. Fernandez-Nieves, V. Vitelli, A. S. Utada, D. R. Link, M. Marquez, D. R. Nelson, and D. A. Weitz, Phys. Rev. Lett. **99**, 157801 (2007).
[16] D. C. Flanders, D. C. Shaver, and H. I. Smith, Appl. Phys. Lett. **32**, 597 (1978).
[17] C. P. Lapointe, T. G. Mason, and I. I. Smalyukh, Science **326**, 1083 (2009).
[18] J. P. Michel, E. Lacaze, M. Goldmann, M. Gailhanou, M. de Boissieu, and M. Alba, Phys. Rev. Lett. **96**, 027803 (2006).
[19] I. I. Smalyukh and O. D. Lavrentovich, Phys. Rev. E **66**, 051703 (2002).
[20] P. Pieranski *et al.*, Physica A (Amsterdam) **194**, 364 (1993).
[21] A. Honglawan, D. A. Beller, M. Cavallaro, R. D. Kamien, K. J. Stebe, and S. Yang, Adv. Mater. **23**, 5519 (2011).
[22] H.-L. Liang, S. Schymura, P. Rudquist, and J. Lagerwall, Phys. Rev. Lett. **106**, 247801 (2011).
[23] T. Lopez-Leon, A. Fernandez-Nieves, M. Nobili, and C. Blanc, Phys. Rev. Lett. **106**, 247802 (2011).
[24] C. C. Ho, A. Keller, J. A. Odell, and R. H. Ottewill, Colloid Polym. Sci. **271**, 469 (1993).
[25] J. A. Champion, Y. K. Katare, and S. Mitragotri, Proc. Natl. Acad. Sci. U.S.A. **104**, 11901 (2007).
[26] D. Armani, C. Liu, and N. Aluru, in *IEEE International MEMS '99: Twelfth IEEE International Conference on Micro Electro Mechanical Systems, Orlando, 1999* (IEEE, New York, 1999), p. 222.
[27] See Supplemental Material at http://link.aps.org/supplemental/10.1103/PhysRevLett.108.207802 for details on how to measure the length of line defects, the derivation of Eq. (1), the rough estimation of the contribution of 3D defects to the 2D model, and more images of droplets.
[28] C. Blanc and M. Kleman, Eur. Phys. J. E **4**, 241 (2001).
[29] C. Blanc and M. Kléman, Eur. Phys. J. B **10**, 53 (1999).
[30] M. Delaye, R. Ribotta, and G. Durand, Phys. Lett. **44A**, 139 (1973).
[31] N. A. Clark and R. B. Meyer, Appl. Phys. Lett. **22**, 493 (1973).
[32] We acknowledge the referee for suggesting that the defects can be created by the instability of dilated smectic layers.
[33] P. G. de Gennes, C.R. Acad. Sci. B **275**, 549 (1972).
[34] P. Boltenhagen, O. D. Lavrentovich, and M. Kléman, Phys. Rev. A **46**, R1743 (1992).
[35] J. B. Fournier, Phys. Rev. E **50**, 2868 (1994).
[36] C. Williams and M. Kléman, J. Phys. (Paris), Colloq. **36**, C1-315 (1975).
[37] M. Kléman and O. D. Lavrentovich, Eur. Phys. J. E **2**, 47 (2000).
[38] F. Nallet and J. Prost, Europhys. Lett. **4**, 307 (1987).
[39] Considering the preference for a larger Burgers vector [2], we assume $d_B \gg \lambda$. However, even when $d_B \sim 2\lambda$, calculated $\gamma \approx 70^\circ$ is almost within the range of experimental data.
[40] P. E. Cladis, J. Phys. (Paris), Colloq. **37**, C3-137 (1976).
[41] P. E. Cladis, Philos. Mag. **29**, 641 (1974).
[42] P. G. de Gennes and P. Pincus, J. Phys. (Orsay, Fr.) **37**, 1359 (1976).
[43] R. Pratibha and N. V. Madhusudana, J. Phys. II (France) **2**, 383 (1992).